NUMERICAL EXPERIMENTS ON SELF-CONTROL OF WALL TURBULENCE BY SURFACE MORPHOLOGY

Peter Lammers
CD-adapco
Nordost Park 3-5, D-90411 Nuremberg, Germany
peter.lammers@de.cd-adapco.com

Jovan Jovanović
Institute of Fluid Mechanics
Friedrich-Alexander University Erlangen-Nuremberg
Cauerstrasse 4, D-91058 Erlangen, Germany
jovan.jovanovic@lstm.uni-erlangen.de

Bettina Frohnapfel
Center of Smart Interfaces
Technische Universität Darmstadt
Petersenstr. 32, D-64287 Darmstadt, Germany
frohnapfel@csi.tu-darmstadt.de

Antonio Delgado
Institute of Fluid Mechanics
Friedrich-Alexander University Erlangen-Nuremberg
Cauerstrasse 4, D-91058 Erlangen, Germany
antonio.delgado@lstm.uni-erlangen.de

ABSTRACT

The self-control of turbulence in wall-bounded flows is considered in pipes of non-circular cross-sections which act to restructure fluctuations towards the limiting state where these must be entirely suppressed. Direct numerical simulations of turbulence in pipes of polygon-shaped cross-sections with straight and profiled sides were performed at a Reynolds number $Re_\tau \simeq 300$ based on the wall shear velocity and the hydraulic diameter. Using the lattice Boltzmann numerical algorithm, turbulence was resolved with up to about 540×10^6 grid points ($8192 \times 257 \times 256$ in the x_1, x_2 and x_3 directions). The first exploratory results show a decrease in the viscous drag around corners, resulting in a reduction of the skin-friction coefficient compared with expectations based on the well-established concept of hydraulic diameter and the use of the Blasius correlation. These findings support the conjecture that turbulence might be completely suppressed if the pipe cross-section is a polygon consisting of a sufficient number of profiled sides of the same length which intersect at right-angles at the corners.

INTRODUCTION

In previous studies carried out by the authors and associates (Jovanović and Hillerbrand, 2005; Jovanović et al., 2006; Lammers et al., 2006; Frohnapfel et al., 2007), the unified theory of skin-friction reduction in turbulent wall-bounded flows was proposed along with the results of its validity using available databases of direct numerical simulations. The starting point in reasoning about the chief mechanism involved in turbulent drag reduction by high polymers, surfactant additives, rigid fibers and riblets including the closely related phenomena observed in strongly accelerated and supersonic flows relied on the role played by the average total energy dissipation $\overline{\Phi}$:

$$\overline{\Phi} = \frac{1}{V}\int_V \underbrace{\nu\left(\frac{\partial \overline{U}_i}{\partial x_j} + \frac{\partial \overline{U}_j}{\partial x_i}\right)\frac{\partial \overline{U}_i}{\partial x_j}}_{\mathrm{I}}\,\mathrm{d}V + \frac{1}{V}\int_V \underbrace{\overline{\nu\left(\frac{\partial u_i}{\partial x_j} + \frac{\partial u_j}{\partial x_i}\right)\frac{\partial u_i}{\partial x_j}}}_{\mathrm{II},\,\varepsilon}\,\mathrm{d}V = \frac{A_w \tau_w U_m}{\rho V}. \qquad (1)$$

The two terms in (1) correspond to direct (I) and turbulent dissipation (II) and their overall contribution to $\overline{\Phi}$ can be evaluated from the work done against the wall shear stress, τ_w, per unit mass of the working fluid, ρV, where A_w is the wetted surface area and U_m is the bulk velocity. An order of magnitude analysis shows that, in turbulent flows at large Reynolds numbers, the largest contribution to $\overline{\Phi}$ is due to turbulent dissipation, ε, which reaches a maximum at the wall and decays away from the wall region. Therefore, a large turbulent drag reduction can be expected if the turbulent dissipation at the wall is minimized, leading to minimization of $\overline{\Phi}$.

By projecting the dynamics of turbulence from the real space into the functional space formed by two scalar invariants, $\mathrm{II_a} = a_{ij}a_{ji}$ and $\mathrm{III_a} = a_{ij}a_{jk}a_{ki}$, of the anisotropy tensor, $a_{ij} = \overline{u_i u_j}/q^2 - 1/3\delta_{ij}$ ($\overline{u_i u_j}$ and q^2 denote the Reynolds stress tensor and its trace, respectively), Jovanović and Hillerbrand (2005) showed that the turbulent dissipation rate must vanish at the wall, $\varepsilon_\mathrm{w} \to 0$ as $x_2 \to 0$, if the velocity fluctuations in the near-wall region satisfy local axisymmetry with invariance to rotation about the axis aligned with the mean flow direction so that the streamwise intensity, $\overline{u_1^2}$, is much larger than in the other two directions along which the intensities are same, $\overline{u_2^2} = \overline{u_3^2}$. This deduction is well supported by available databases from direct numerical simulations and is in close agreement with results of direct numerical simulations with

forced boundary conditions which display a high drag reduction when turbulence in the viscous sublayer is manipulated to tend towards the one-component limit in an axisymmetric fashion (Frohnapfel et al., 2007).

THE CROSS-SECTION GEOMETRY

In order to elucidate the surface topology which promotes a large viscous drag reduction, we shall first examine the statistical features of turbulence in a fully developed flow through a straight duct of square cross-section shown in figure 1 (center). It is well known (Schlichting, 1968) that secondary flows appear near duct corners known as Prandtl's vortices of the second kind, which cannot develop if the flow assumes the laminar state. These counter-rotating vortices are formed due to interaction of the high-speed fluid, originating from the core region, as it is transported towards the duct corners where it is forced to split sidewise along both walls.

The flow development along the wall normal bisector shown in figure 1 (center-bottom-right) is weakly influenced by side walls and the turbulence statistics resemble trends observed in the plane channel flow. The trajectory in the anisotropy-invariant map shows that the data corresponding to the region of the viscous sublayer lie along the two-component state (2C) mid-way between the two-component isotropic state (2C-iso) and the one-component state (1C). Away from the wall region, the trajectory shows a pronounced tendency for turbulence to approach the axisymmetric state, which is reached at the duct centerline. In the viscous sublayer, the velocity fluctuations normal to the wall are suppressed, $u_2 \approx 0$, so that fluid motions are constrained to planes parallel to it (x_1, x_3) having only streamwise, u_1, and spanwise, u_3, velocity components. Such a flow structure allows the development of turbulent dissipation which reaches a maximum at the wall and decay away from it following the local equilibrium between the turbulence production and turbulent dissipation. As a consequence of spatial variation of turbulence statistics, the mean velocity profile is almost uniform in the core region and exhibits a steep gradient at the wall (see figure 1, center-top-left).

The evolution of turbulence along corner bisectors shown in figure 1 (center-top-right) is strongly influenced by side walls forcing normal and spanwise velocity components to develop in the same fashion. Both of these velocity components are suppressed near walls and the trajectory in the anisotropy-invariant map shows that turbulence is axisymmetric along the entire corner bisector starting from the wall at the one-component limit (1C) up to the duct centerline where turbulence is almost isotropic. The structure of the viscous sublayer is altered in such a way that turbulent dissipation cannot develop at the wall and is reduced significantly away from it compared with the corresponding distribution along the wall normal bisector. As a result of such spatial development of turbulence, the mean velocity profile shows a tendency for flow relaminarization with a significant reduction in the slope at the wall (see figure 1, center-top-left). The distribution of the wall shear stress shown in figure 1 (center-bottom-left) reflects these trends and displays consequential changes in the turbulence structure along various cross-sections of the duct.

The variation of turbulence statistics along two different bisectors of the duct flow provides useful hints on how turbulence anisotropy, dissipation rate, mean flow and the wall shear stress can be altered rationally. This immediately suggests that if we intend to achieve a large viscous drag reduction, the cross-section geometry has to be composed of a large number of corner bisectors in order to ensure that axisymmetry in turbulence prevails not only near the wall but also across the entire flow domain.

As an initial guess, polygon-shaped cross-sections, shown in figure 1 (left), consisting of a large number of straight sides between corners, might be considered. For a large number of corners, such configurations asymptotically approach the circle and we may argue, in the context of the previous discussion, that the mechanism responsible for the remarkable stability of circular pipe flows at very large Reynolds numbers is due to increased anisotropy in the disturbances induced by the surface curvature. Some supporting evidence may be added in respect to the above issue: (i) examination of the transport equations for the Reynolds stresses and anisotropy-invariant mapping of turbulence in circular pipe flows using DNS databases reveal higher anisotropy in the viscous sublayer compared with plane channel flows (Pashtrapanska, 2004); (ii) experiments performed in circular pipes confirmed an increase in the transition Reynolds number with increasing surface curvature, e.g. decreasing the pipe diameter (Haddad, 2009); (iii) analysis of the experimental and numerical data shows that the turbulent Reynolds number, R_λ, in pipe flows ($R_\lambda \approx 1.996 Re_\tau^{1/2} + 0.108$) is lower than in plane channel flows ($R_\lambda \approx 2.971 Re_\tau^{1/2} - 6.618$), which implies a reduction in the spectral separation, L/η_K, due to the surface curvature effect (Jovanović and Pashtrapanska, 2004).

For a finite number of corner bisectors, simple polygon configurations with straight sides between corners are not appropriate since these configurations do not ensure axisymmetry of turbulence near the wall. In order to force axisymmetry, polygons with profiled side walls intercepting at right-angles are suggested, as shown in figure 1 (right), as the simplest means to obtain the desired turbulence structure which promotes high drag reduction.

COMPUTATIONAL DOMAIN AND NUMERICAL METHOD

Computational domain

The simulated flow configurations and the coordinate system employed are shown in figure 2.

For wall-bounded flows the velocity scale u_τ is related to the streamwise pressure gradient $\partial\overline{P}/\partial x_1$ through the mean momentum equation $u_\tau = [0.25(D_h/\rho)(\partial\overline{P}/\partial x_1)]^{1/2}$, where D_h is the hydraulic diameter defined in terms of the cross-section area, A, and the wetted perimeter, O, as $D_h = 4A/O$. For our simulations the Reynolds number Re_τ, based on u_τ and the hydraulic diameter D_h, was fixed to the value $Re_\tau = D_h u_\tau/\nu = D_h^+ \simeq 300$.

For the geometries shown in figure 2, the flow is homogeneous in the streamwise direction so that periodic boundary conditions were used in this direction. Using an equidistant cartesian grid with $8192 \times 257 \times 256$ points in the x_1, x_2 and x_3 directions, the non-dimensional grid spacing was $\Delta x_i^+ = 1.17$. The estimated value of the Kolmogorov length scale, $\eta_K^+ = (0.25 Re_\tau u_\tau/U_m)^{1/4}$, obtained from the average

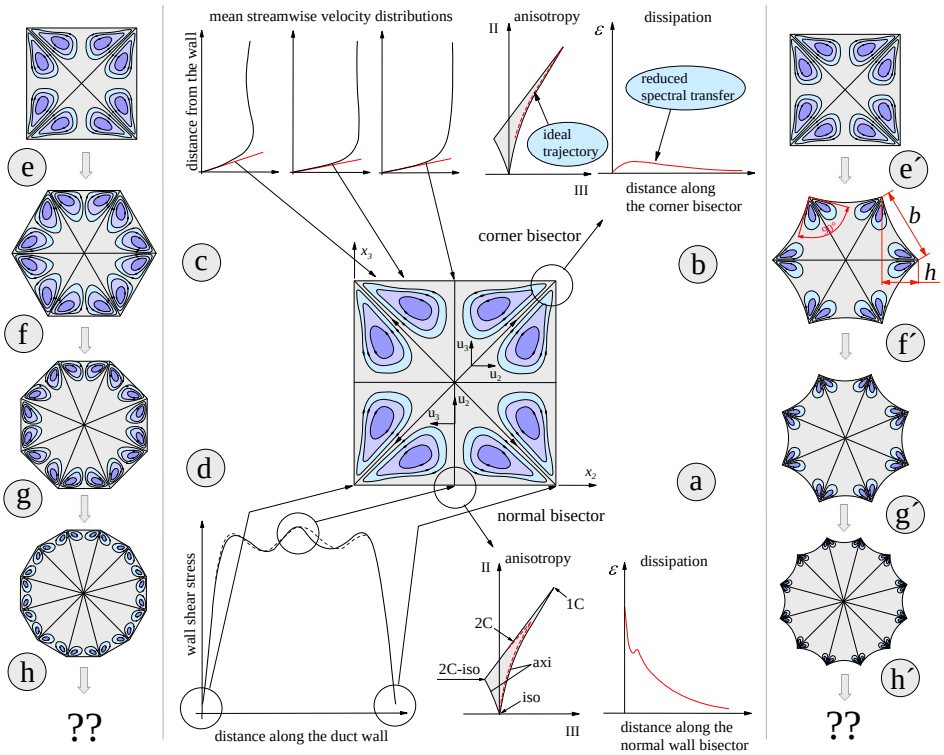

Figure 1. The structure of turbulence in a square duct flow (center) and in pipes of non-circular cross-sections (left and right). (a) Along wall-normal bisectors, the turbulence structure has the form common for wall-bounded flows. (b) Along corner bisectors, turbulence approaches the ideal trajectory in the anisotropy-invariant map, resulting in a significant reduction in the dissipation (ε) and spectral transfer with formation of quasi-deterministic highly elongated streaks induced by secondary motions.(c),(d) Close to corners, reduced spectral transfer results in a noticeable reduction in the wall shear stress. (e)-(h$^{'}$) Possible, polygonal or similar, flow configurations of pipe cross-sections with a finite number of corner bisectors: in such configurations, turbulence might be self-suppressed whenever secondary motions start to appear.

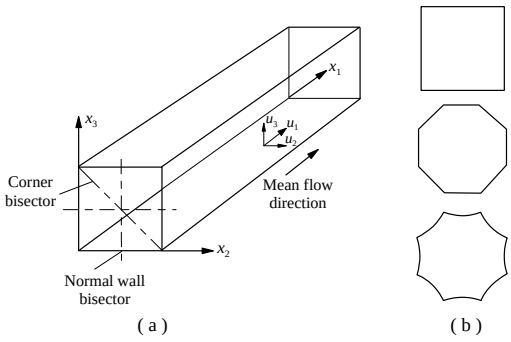

Figure 2. Computational domain with coordinate system, *(a)*, and simulated cross-section configurations, *(b)*.

dissipation rate across the entire flow domain per unit mass of the working fluid was $\eta_K^+ \approx 1.5$. The grid resolution $\Delta x_i^+ \simeq 0.78\eta_K^+$ was therefore fine enough to resolve all dissipation and obtain reliable results for first- and second-order turbulence statistics.

Numerical method

The choice of the numerical method was motivated by the demand for an algorithm with small computing costs per grid point and time step. In this respect, the lattice Boltzmann method (LBM) was a logical and attractive choice. The method utilizes the fact that information on the velocity $\vec{U}$ and the pressure p of a viscous fluid can be obtained by solving a kinetic equation for a one-particle distribution function f instead of Navier-Stokes equations directly. The function $\tilde{f} = \tilde{f}(\vec{\xi},\vec{r},t)$ depends on the molecular velocity $\vec{\xi}$, the position in space $\vec{r}$ and the time $\tilde{t}$. The hydrodynamic quantities are obtained from the moments of the distribution function. A very popular kinetic model is described by the Boltzmann equation together with the so-called Bhatnagar-Gross-Krook (BGK) ansatz for the collision operator

$$\left(\partial_{\tilde{t}} + \vec{\xi}\cdot\vec{\nabla}_{\vec{r}} + \vec{\mathscr{F}}\cdot\vec{\nabla}_{\vec{\xi}}\right)\tilde{f}(\vec{\xi},\vec{r},\tilde{t}) = -\frac{\tilde{f}(\vec{\xi},\vec{r},\tilde{t}) - \tilde{f}^{eq}(\vec{\xi},\vec{r},\tilde{t})}{\lambda}, \tag{2}$$

where $\vec{\mathscr{F}}$ is the external force. The function $\tilde{f}^{eq}$ corresponds to the equilibrium (Maxwell-Boltzmann) distribution and λ is a relaxation time. This equation is discretized in time and space. Additionally, a finite set of velocities $\vec{c}_i$ for $\vec{\xi}$ has to be defined. As a result of discretization, the following non-

dimensional equation is obtained:

$$f_i(\vec{x}+\vec{c}_i,t+1)-f_i(\vec{x},t)=-\omega(f_i(\vec{x},t) - f_i^{eq}(\rho,\vec{U}+\tfrac{\vec{\mathscr{E}}}{2\rho},\vec{x},t))\left(f_i(\vec{x},t)-f_i^{eq}(\vec{x},t)\right) +3t_p\frac{2-\omega}{2}\vec{c}_i\cdot\vec{\mathscr{E}}, \quad (3)$$

where f_i is the distribution function of the velocity $\vec{c}_i$. The force density $\vec{\mathscr{E}}$ is given by the pressure gradient according to $\vec{\mathscr{E}}=\vec{\nabla}p$, whereby $\mathscr{E}_1$ is the only remaining component in our case. The macroscopic behavior of equation (3) is obtained by a Chapman-Enskog procedure together with a Taylor expansion of the Maxwell-Boltzmann equilibrium distribution for small velocity (small Mach number). For this equilibrium distribution

$$f_i^{eq}=t_p\rho\left\{1+\frac{c_{i_\alpha}U_\alpha}{c_s^2}+\frac{U_\alpha U_\beta}{2c_s^2}\left(\frac{c_{i_\alpha}c_{i_\beta}}{c_s^2}-\delta_{\alpha\beta}\right)\right\} \quad (4)$$

it can be shown that the Mach number must be $|u/c_s|\ll 1$ in order to satisfy the incompressible Navier-Stokes equations. The parameters t_p and $p=\|\vec{c}_i\|^2$ depend on the discretization of the molecular velocity space. For the present simulations, a three-dimensional model with 19 velocities $\vec{c}_i$, $i=0,\ldots,18$ (D3Q19) was employed. The D3Q19 model has the parameters $t_0=1/3$, $t_1=1/18$ and $t_2=1/36$. Our implementation of LBM was validated against the well-resolved pseudo-spectral simulation of a plane channel flow at $Re_\tau\approx 180$. Results of lattice Boltzmann simulation reported by Lammers et al. (2006) confirm that profiles of the mean velocity, root-mean-square velocity fluctuations, turbulent shear stress and the balance of the turbulence kinetic energy equation agree closely with the results of Kim et al. (1987).

RESULTS

Turbulent flow through a pipe of square cross-section

In order to produce the desired componentality of the velocity fluctuations by cross-section geometry which leads to the realization of axisymmetric turbulence in the near-wall region, the authors first performed simulation of turbulence in a pipe of square cross-section. It was expected that in such a configuration turbulence will reach the axisymmetric state along corner bisectors and tend towards the one-component state at the wall. By evaluating the turbulence statistics in the region between the wall normal and corner bisectors, it was possible to confirm the results of the theoretical considerations and show that the axisymmetric state of wall turbulence leads to a large reduction in the wall shear stress in the region around corners.

Figure 3 shows distributions of the mean flow, all components of the Reynolds stress tensor and the turbulence anisotropy across one of the eight octants of a square cross-section. These results provide a demonstration for desired modifications of turbulence induced by the presence of the side walls which intersect at right-angles. Distributions of the Reynolds stresses reveal that turbulence reaches the axisymmetric state in the close vicinity of the corners with invariance to rotation for 90° about the axis aligned with the mean flow direction. At corners turbulent stresses satisfy the relations which hold for such a form of axisymmetric turbulence: $\overline{u_1^2}>\overline{u_2^2}=\overline{u_3^2}$ and $|\,\overline{u_1u_2}\,|=|\,\overline{u_1u_3}\,|$. Trajectories in the anisotropy-invariant map reflect these trends and confirm that anisotropy increases as corners are approached so that turbulence along the corner bisector follows the right-hand boundary of the anisotropy map which represents axisymmetric turbulence with the one-component state located at the wall. Approaching corners, slopes of the turbulent stresses and of the mean flow continuously decrease at the wall. This trend supports the expectation that a decrease in the turbulent dissipation rate at the wall, ε_w, leads to a lower value of the integral (1) and therefore a decrease in the wall shear stress, τ_w.

Turbulent flow through pipes of the polygon cross-sections

In reasoning about the cross-section configurations which would notably increase the anisotropy of turbulence along the entire wetted perimeter, which would than prevail across the whole flow domain, polygon cross-section geometries composed of profiled sides intersecting at right-angles at the corners are suggested. For such configurations with large number of corners simulation is, however, very demanding owing to the fine resolution needed to capture the evolution of the flow structures near corners. These structures are expected to have a significant impact on the viscous drag. Using the very efficient lattice-Boltzmann algorithm which currently operates extremely well exclusively on the equidistant grids, cross-section configurations with only few corners can be simulated with reasonable effort. Therefore, an attempt was made to obtain first exploratory results by conducting two simulations of turbulence development in pipes of octagon cross-sections having straight and profiled sides. By studying differences in the flow development through such pipes, it is possible to extract effects expected to prevail for a large number of corners.

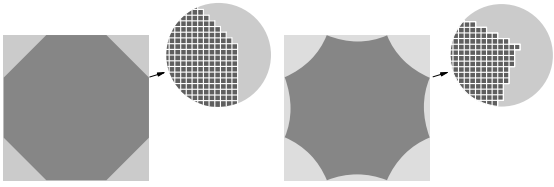

Figure 4. Discretisized cross-section geometries of turbulent pipe flow: octagon with straight sides (left) and octagon with profiled sides (right).

The simulated cross-section geometries are shown in figure 4. Owing to uniform discretization of the flow domain using equidistant cartesian grids, the wall boundaries are smooth within the grid resolution, $\Delta x_i^+=1.17$, and symmetry between various orthants of the octagon cross-sections is preserved within an equivalent degree of approximation.

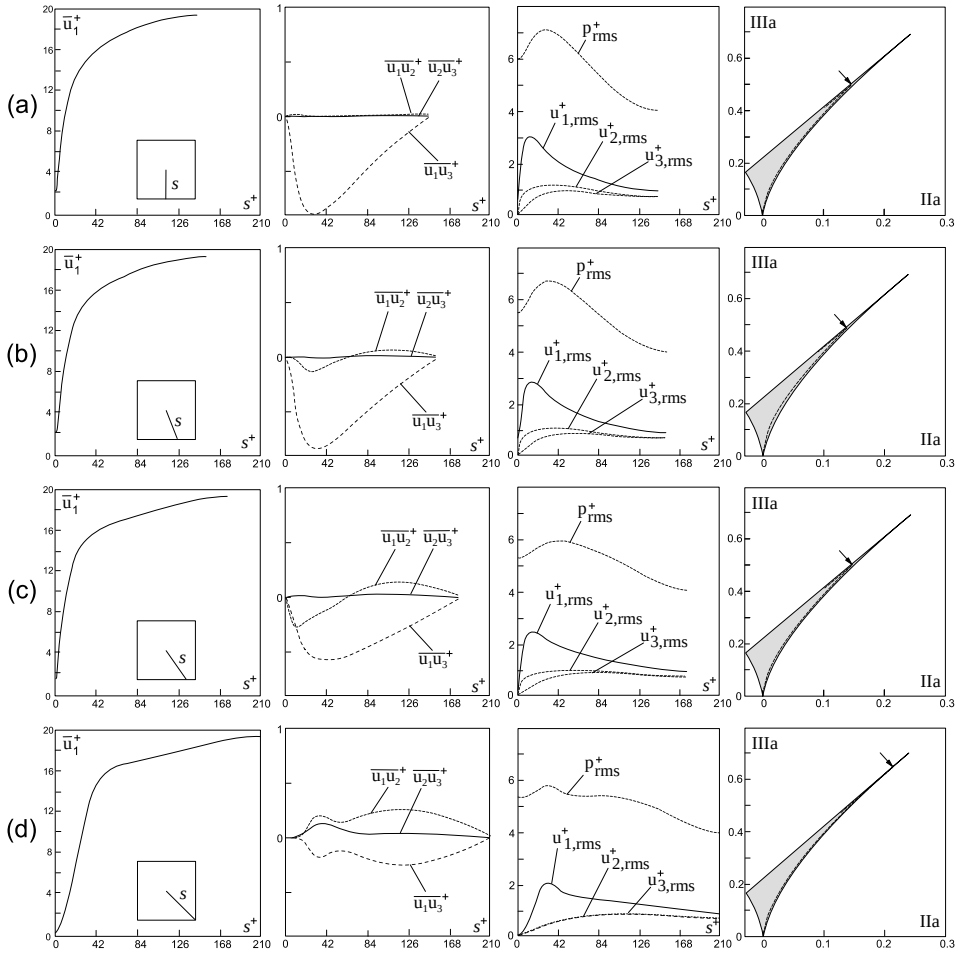

Figure 3. The structure of turbulence in a pipe flow of square cross-section at $Re_m = D_h U_m/\nu \simeq 4362$. The profiles of the mean velocity, Reynolds stresses and turbulence anisotropy in the region between the normal, *(a)*, and corner bisectors, *(d)*. Arrows indicate the maximum value of turbulence anisotropy. These data are non-dimensionalized by the wall friction velocity calculated from the pressure gradient along the pipe and plotted versus the normalized distance starting from the pipe centerline up to the wall, $s^+ = su_\tau/\nu$.

Comparisons of the flow development in pipes of octagon cross-sections with straight and profiled sides are shown in figure 5. These results display essential differences in the flow development in the region around corners which are expected to play a major role in turbulent drag reduction and potentially also in self-stabilization of the laminar boundary layer development at large Reynolds numbers.

The computed trajectories in the anisotropy-invariant maps reveal that anisotropy increases along the profiled sides of the octagon cross-section and reaches at the corners almost the one-component limit. This trend in turbulence anisotropy is reflected in distributions of the mean velocity which display a continuous reduction of the wall shear stress as corners are approached. These results correspond to a Reynolds number of $Re_m = D_h U_m/\nu \simeq 4386$ and a skin friction coefficient of $c_f = \tau_w/(0.5U_b^2\rho) = 2(Re_\tau/Re_m)^2 = 9.35\times10^{-3}$. This value of c_f is 3.9% lower than the prediction based on the well-known Blasius correlation $c_f = 0.0791 Re_m^{-1/4}$.

Across the octagon cross-section with straight sides there is no noticeable increase in anisotropy as observed in the cross-section with profiled sides and consequently no trend in reduction of the wall shear stress at and near corners. These results correspond to a Reynolds number of $Re_m \simeq 4277$ and a skin friction coefficient of $c_f \simeq 9.838\times10^{-3}$. For this cross-section configuration, the value of c_f obtained is slightly higher than that deduced from the Blasius correlation.

CONCLUSIONS

An attempt was made, on purely theoretical grounds, to derive the cross-section geometry of a fully developed pipe flow which forces near-wall turbulence to approach the limiting state where it must be completely suppressed. Following invariant analysis of turbulence, a cross-section geometry was suggested in the form of polygon with profiled sides intersecting at right-angles at the corners. A description is provided of the manner in which the proposed geometry alters near-wall turbulence leading to a significant turbulent drag reduction.

In order to support the proposed concept of flow control,

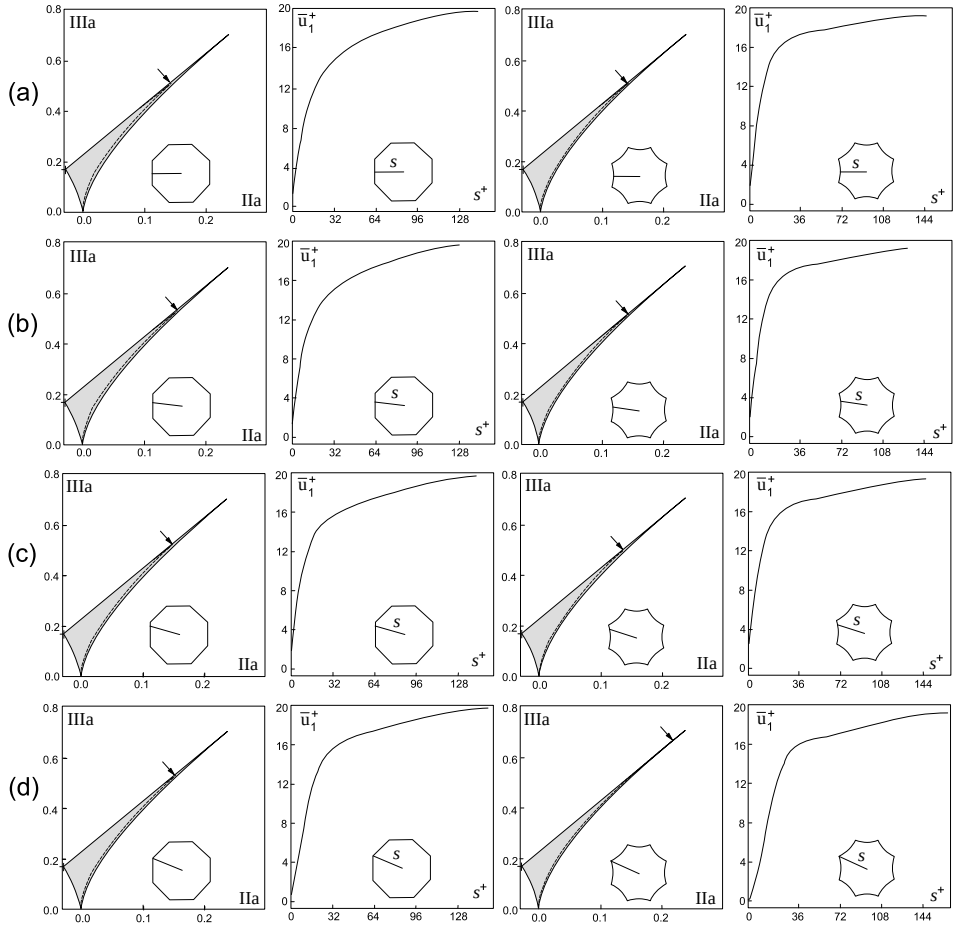

Figure 5. The structure of turbulence in pipes with octagon shape cross-sections. Comparisons of trajectories in the anisotropy-invariant maps and profiles of mean velocity in the region between the wall normal bisector and the corner bisector for an octagon with straight sides against an octagon with profiled sides. Arrows indicate the maximum level of the turbulence anisotropy.

direct numerical simulations of turbulence in pipes of non-circular cross-sections were performed using the lattice Boltzmann numerical method. First exploratory results confirmed that the chief mechanism responsible for the turbulent drag reduction is related to the ability of the profiled surface to increase the anisotropy in the velocity fluctuations very close to the wall. It is hoped that further simulation work following the concept outlined in this paper will bring additional evidence in closer accord with the theoretical expectations.

REFERENCES

Haddad, K.E., 2009, Development of special test rigs and their application for pulsating and transitional flow investigations, PhD Thesis, Friedrich-Alexander-Universität Erlangen-Nürnberg.

Frohnapfel, B., Lammers, P., Jovanović, J., and Durst, F., 2007, "Interpretation of the mechanism associated with turbulent drag reduction in terms of anisotropy invariant", Journal of Fluid Mechanics, Vol. 577, pp. 457- 466.

Jovanović, J. and Pashtrapanska, M., 2004, "On the criterion for the determination transition onset and breakdown to turbulence in wall-bounded flows", Journal of Fluids Engineering, Vol. 126, pp.626- 633.

Jovanović, J., and Hillerbrand, R., 2005, "On peculiar property of the velocity fluctuations in wall-bounded flows", Thermal Science, Vol. 9, pp. 3- 12.

Jovanović, J., Pashtrapanska, M., Frohnapfel, B., Durst, F., Koskinen, J., and Koskinen, K., 2006, "On the mechanism responsible for turbulent drag reduction by dilute addition of high polymers: theory, experiments simulations and predictions", Journal of Fluids Engineering, Vol. 128, pp. 626- 633.

Kim, J., Moin, P., and Moser, R., 1987, "Turbulence statistics in fully developed channel flow at low Reynolds number", Journal of Fluid Mechanics, Vol. 177, pp.133- 166.

Lammers, P., Jovanović, J., and Durst, F., 2006, "Numerical experiments on wall turbulence at low Reynolds numbers", Thermal Science, Vol. 2, pp. 33- 62.

Pashtrapanska, M., 2004, Experimentelle Untersuchung der turbulenten Rohrströmungen mit abklingender Drallkomponente, PhD Thesis, Friedrich-Alexander-Universität Erlangen-Nürnberg.

Schlichting, H., 1968, *Boundary-Layer Theory.* 6th edn., McGraw-Hill, New York.